Journal of Molecular Structure 1373 (2026) 146670

Contents lists available at ScienceDirect

Journal of Molecular Structure

journal homepage: www.elsevier.com/locate/molstr

Exploring the Biomaterial Potential of a Naphthalene-based Schiff Base through Protein Binding, Molecular Docking, MD Simulation, and Swiss-ADME analysis

Kathiravan Poornima [a], Venkatesan Srinivasan [a,*], Renganathan Senthil [b], Mohandass Yeshwanth Sree [c], Pushparaj Sandhyadevi [c], Kannan Ramamurthy [d,*]

[a] Department of Chemistry, Vel Tech Rangarajan Dr.Sagunthala R&D Institute of Science and Technology, Avadi, Chennai 600 062, Tamil Nadu, India
[b] Department of Bioinformatics, School of Life Science, Vels Institute of Science, Technology & Advanced Studies (VISTAS), Pallavaram, Chennai 600 117, Tamil Nadu, India
[c] Department of Chemistry, Agurchand Manmull Jain College, Meenambakkam, Chennai, Tamil Nadu 600 061, India
[d] Department of Chemistry, Vels Institute of Science, Technology & Advanced Studies (VISTAS), Pallavaram, Chennai 600 117, Tamil Nadu, India

ARTICLE INFO

Keywords:
Schiff base
HOMO-LUMO
Protein binding
Molecular docking
MD simulation
Swiss-ADME

ABSTRACT

Phenolic-based Schiff bases are highly interesting in biological applications due to their enhanced stability, strong metal-chelating ability, and capacity to form hydrogen bonds and electrostatic interactions with biomolecules, which enhance their notable pharmacological and bioactive effects. A Schiff base ligand, (E)-1-(((2-aminophenyl)imino)methyl)naphthalen-2-ol (**OPN**) was derived from 2-hydroxy-1-naphthaldehyde and o-phenylenediamine. **OPN** was thoroughly characterized using standard spectroscopic and microscopic techniques, such as FT-IR, NMR and HR-MS analysis. **OPN** was further investigated using density functional theory (DFT) calculations to determine the HOMO–LUMO energy levels, and the derived global reactivity parameters provided valuable insights into its chemical reactivity, kinetic stability, and electronic properties. Fluorescence quenching analysis was used to check the binding interaction between bovine serum albumin (BSA) and **OPN**. The strong binding interaction was confirmed by the obtained quenching rate constant (2.79×10^{13} M^{-1} s^{-1}) and a moderate binding constant (7.14×10^{5} M^{-1}). Further, we performed the fluorescence quenching analysis at different temperatures and confirmed that the quenching is due to static quenching. The experimental results related to molecular docking analysis indicate that **OPN** binds strongly within the active sites of BSA. Moreover, molecular dynamics simulations revealed that the BSA-**OPN** complex remained structurally stable for up to 50 ns, indicating a stable, energetically favourable binding interaction. Swiss-ADME analysis was performed to assess the pharmacokinetic and drug-likeness characteristics of **OPN**. Overall, this work highlights the significant binding ability of the synthesized **OPN** with protein, suggesting its potential applicability towards biological applications.

1. Introduction

Schiff bases are a widely studied, simple and significant class of organic ligands. Generally, Schiff bases are synthesized by a simple condensation technique by using aromatic aldehydes/ketones with amines to produce the azomethine (-C = N) group. Their popularity as ligands stems from their simple synthesis, high selectivity for the central metal ion [1], versatile synthetic methods [2], structural diversity [3], and extensive biological applications [4]. In addition, compounds derived from Schiff base have garnered considerable interest from researchers due to their strong chelating ability towards metal ions [5–7]. These Schiff bases and their complexes play a crucial role in antitumor activity [8], antioxidative activities [9,10], and photophysical properties [9,11] and are used as vital components in drugs [12–14]. Additionally, Schiff bases containing phenol in their ligand structure are of significant medicinal value. Drug compounds developed with a phenolic moiety show an excellent biological efficacy, such as antioxidative [15], antimutagenic, and anticarcinogenic properties [16]. Introducing a hydroxyl group into the molecule increases its water solubility and enhances its interface with bio-active molecules [17]. The

* Corresponding authors.
E-mail addresses: vasan15790@gmail.com (V. Srinivasan), kramchem1988@gmail.com (K. Ramamurthy).

https://doi.org/10.1016/j.molstruc.2026.146670
Received 24 March 2026; Received in revised form 20 May 2026; Accepted 25 May 2026
Available online 26 May 2026

phenoxy radicals are effectively produced from metal-coordinated phenol moieties, and are important in enzymes (galactose oxidase and glyoxal oxidase) [18]. Literature clearly reports that Schiff bases and phenolato-containing compounds interacting with serum proteins have been documented [16,19–22] Moreover, Al-Harrasi and co-workers reported that hydrazone-based Schiff base derivatives exhibit strong interactions with enzymes, highlighting their potential as promising candidates for drug development in medicinal chemistry [23–25].

Fluorescence spectral analysis of proteins plays a crucial role in their bio-chemical applications in cells [26,27]. The basic fluorescence of a protein originates from the following amino acids like tyrosine, phenylalanine and tryptophan. Tryptophan exhibits a strong fluorescence and is highly sensitive to changes in the local environment [28]. Generally, serum albumin plays a crucial role in the blood plasma and helps to maintain osmotic pressure [29]. While numerous transport proteins are present in blood plasma, albumin uniquely and reversibly binds and transports various ligands [30]. During intravenous administration, serum proteins and DNA are primary targets for drugs [31]. Albumins can bind drugs and other bioactive molecules [29,30], creating important attention in the study of their interactions. Bovine Serum Albumin (BSA) is structurally similar to human serum albumin (HSA), and is a well-characterized, plentiful, as well as cost-effective serum albumin [32,33]. The properties mentioned above make BSA a valuable tool for studying drug-protein interactions, as its strong, specific binding to drug/small molecules/dyes can facilitate drug delivery. BSA also acts as a distributor and carrier for various exogenous and endogenous ligands [34,35]. The interaction studies comprise multi-spectroscopic and molecular simulation approaches with theoretical calculations [36–38]

The purpose of this study is to describe the molecular structure of a naphthalene-based Schiff base using both experimental and theoretical methods and to investigate its biological characteristics. From that, we have synthesized the naphthalene-based Schiff base using a simple stirring technique and thoroughly characterized. Further, DFT calculation was used to optimize the **OPN** structure and calculate the global reactivity parameters. The binding interaction analysis with BSA was performed using **OPN**, which showed strong binding affinity between **OPN** and BSA. Further, the exact binding sites were identified via molecular docking study, and the stability of the binding interaction was confirmed by MD simulation. Additionally, Swiss-ADME was used to assess the drug-likeness and pharmacokinetics of the **OPN** compound, confirming satisfactory absorption and bioavailability.

2. Experimental section

2.1. Materials and methods

Ortho-phenylenediamine (≥98.0%) and 2-hydroxy-1-naphthaldehyde (≥99.9%) were obtained from BLD Pharma and Sigma Chemicals, India. All the spectral measurements were performed using double-distilled water. Reagents and chemicals are used without any additional purification. BSA (≥98%) was purchased from Sigma Chemicals, India.

Infrared spectra were obtained on an Apodization: Happ-Genzel FT-IR spectrophotometer (4000–650 cm^{-1}). High-resolution mass spectra (EI-HRMS) were recorded on a XEVO-G2-XS-QTOF mass spectrometer. ^{1}H NMR and ^{13}C NMR spectra were recorded on a Bruker AV III 500 MHz NMR. The solvent used for the NMR analysis was DMSO-d_6, and tetramethylsilane (TMS) was used as the internal standard. An Agilent 8453 diode-array spectrophotometer and a Hitachi F-4500 spectrofluorometer were used to conduct photophysical analyzes. Elemental analysis of the compound was measured by using ORGANIC: LECO Truspec Micro CHNS/O analyzer.

2.2. Synthesis of (E)-1-(((2-aminophenyl) imino) methyl) naphthalen-2-ol (OPN)

To a solution of ortho-phenylenediamine (1 mmol) in ethanol (20 mL), 2-hydroxy-1-naphthaldehyde (1 mmol) was added, and the mixture was stirred at room temperature for 6 h (Scheme 1, Table 1). After the reaction was complete (monitored by TLC), the solvent was removed under vacuum, affording the naphthalene-based Schiff base as an orange solid. Product Yield: 85%, m.p 148–150 °C. IR (ν in cm^{-1}): 1602 (imine C = N), 3360 (-NH), 3466 (-OH). ^{1}H NMR(500 MHz, DMSO-d_6): δ 6.83–6.85 (m, 2 H), 7.08–7.10 (m, 3 H), 7.37 (t, $J = 7.5$ Hz, 1 H), 7.47 (t, $J = 7.7$ Hz, 1 H), 7.56 (d, $J = 7.9$ Hz 1 H), 7.83 (d, $J = 9.0$ Hz, 1 H), 8.51(d, $J = 8.5$ Hz, 1 H) 9.60 (s, 1 H), 15.66 (s, 1 H). ^{13}C NMR (500 MHz, DMSO-d_6): δ 167.6, 156.1, 142.2, 136.1, 133.3, 132.1, 129.4, 128.1, 127.3, 123.8, 121.6, 120.9, 119.3, 119.6, 117.7, 116.3, 109.7. ESI-MS TOF *m/z* calcd for $C_{17}H_{14}N_2O$: 262.1106. Found: 263.1028 $[M + H]^+$. Elemental analysis Calcd ($C_{17}H_{14}N_2$): C (77.84%), H (5.38%), N (10.68%), O (6.10%), Found: C (77.81%), H (5.41%), N (10.63%).

2.3. Theoretical analysis

The electronic and molecular properties of the synthesized **OPN** was investigated using Density Functional Theory (DFT) calculations performed with Gaussian 09 software. Geometry optimization of the conformers was carried out employing the B3LYP functional in combination with the 6–31G(d,p) basis set [39]. Geometry optimization was performed in the gas phase without explicit solvent correction. The optimized structure of the **OPN** was visualized using the GaussView 6.0 molecular visualization software. Furthermore, the pharmacokinetic properties, including Absorption, Distribution, Metabolism and Excretion (ADME), were evaluated using the SwissADME web tool, a freely accessible online http://www.swissadme.ch/.

2.4. Protein binding and molecular docking analysis

Herein, we chose BSA as a model protein for binding interaction studies. So, we prepared the BSA stock solution (1%) in phosphate buffer (pH 7.2) and calculated the BSA concentration by spectrophotometry ($\varepsilon_{280} = 44{,}000\ M^{-1}\ cm^{-1}$) [40]. 1 mM concentration of **OPN** was prepared by DMSO, and further, the stock solutions were used for the spectral measurements. The absorption and fluorescence analysis were conducted, and quenching experiments were performed between 290–560 nm (excitation 285 nm). Furthermore, molecular docking analysis was performed to identify specific binding sites and simulate interactions. Herein, the docking results were obtained using CB-Dock software and visualized with Biovia Discovery Studio. The 3D structure of BSA was obtained from the Protein Data Bank (PDB ID: 4F5S). The selected docking cavity was defined with grid center coordinates of (49.2, 21.9, 93.4) and box dimensions of 35 Å × 21 Å × 21 Å.

2.5. MD simulation studies

Combining GROMACS and the CHARMM36 force field, all-atom molecular dynamics (MD) simulations of the synthesized ligand molecule with BSA were carried out. Employing visualization programs like Pymol or VMD, the structure was processed to exclude redundant molecules like ligands, crystallographic water, or multiple conformations. The topology files were generated by choosing a suitable force field using GROMACS's pdb2gmx module. A cubic box with an adequate buffer distance from the solute has subsequently used to establish the simulation box. In order to neutralize the system and replicate physiological ionic strength, ions were added by genion after the system had been solvated using solvate. Energy minimization is used to remove steric conflicts and to enhance geometry. There are two stages to achieving equilibrium. NVT Equilibration: The temperature, volume, and particle count of the system are all kept constant. Thermal

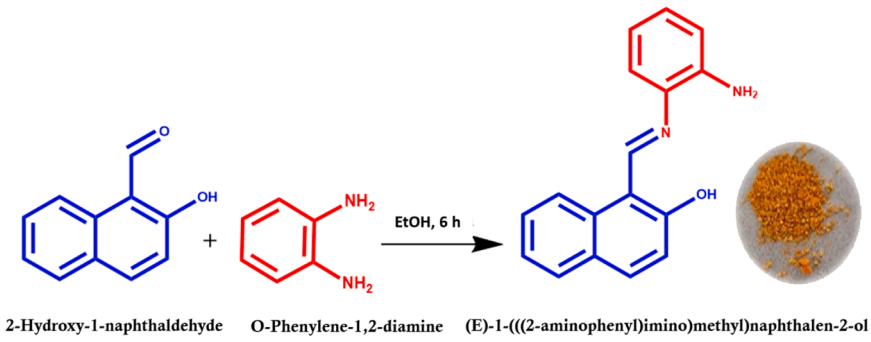

Scheme 1. Synthesis procedure of **OPN**.

Table 1
SMILES String of starting materials and compound (**OPN**).

Compound name	Structure	SMILES String
2-hydroxy-1-naphthaldehyde	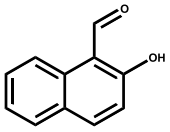	Oc1ccc2ccccc2c1C=O
O-phenylene-1,2-diamine	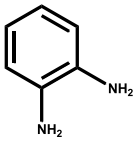	Nc1ccccc1N
(E)-1-(((2-aminophenyl) imino) methyl) naphthalen-2-ol	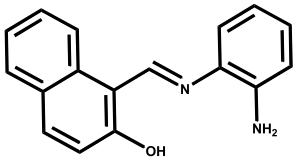	Nc1ccccc1\N = C\c1c(O)ccc2ccccc12

fluctuations are stabilized by applying temperature coupling. NPT Equilibration: For the purpose of density adjustment and pressure stability, the system was further balanced under constant particle counts, pressures, and temperatures. The final production MD run was executed under continuous pressure (NPT ensemble) for 50 nanoseconds (ns). Long-range electrostatics were addressed utilizing the Particle Mesh Ewald (PME) method, and by constraining all covalent bonds, the LINCS algorithm enabled a 2-fs integration timestep [41]. Non-bonded contacts were terminated at 10 Å using the Verlet cutoff method. Trajectory analyses, including radius of gyration (Rg), root mean square fluctuation (RMSF) and root mean square deviations (RMSD), were computed using the integrated GROMACS tools. Conformational dynamics and binding stability were assessed by tracking significant intermolecular distances between the ligand molecules and BSA residues using the XMgrace and plotting tools [42,43]

3. Results and discussions

3.1. Synthesis and characterization

Schiff-base ligands play a significant role in photophysical and biological applications. As a result, we envisioned to synthesize a novel Schiff base (E)-1-(((2-aminophenyl)imino)methyl)naphthalen-2-ol (**OPN**) using a one-pot synthesis process followed by ortho-phenylenediamine and 2-hydroxy-1-naphthaldehyde in ethanol in the presence of a few drops of anhydrous acetic acid. The final compound was thoroughly characterized by FT-IR, ^{1}H & ^{13}C NMR, mass spectral and elemental analysis and displayed in **Figures S1-S3**. The FT-IR spectrum of **OPN** (**Figure S1**) exhibited a characteristic band at 1520 cm^{-1}, attributed to the C = N stretching vibration, confirming imine formation. A broad absorption band observed in the region 3466 cm^{-1} corresponds to the phenolic –OH group, while the N–H stretching vibration appeared at 3360 cm^{-1}. The mass spectrum **(Figure S4)** of the synthesized **OPN** exhibited a prominent molecular ion peak at m/z = 263.1028 $[M + H]^{+}$, which is in good agreement with the calculated exact mass within acceptable mass accuracy limits for TOF-MS analysis. Further, we performed the elemental analysis, which also supported the molecular composition of the synthesized naphthalene derivative. The synthesized **OPN** is structurally distinguished from previously reported Schiff base analogues by the presence of a naphthalene framework coupled with a phenylene diamine moiety. This combination of the structure introduces extended conjugation and a hydroxyl group present in the ortho position, facilitating intramolecular hydrogen bonding. It leads to an increase in the stabilization molecular planarity of the imine structure. These kinds of intramolecular interactions are known to significantly influence the electronic properties and binding behaviour of Schiff bases. The above-discussed results clearly revealed that the presence of significant functional groups is expected to significantly affect the interaction of **OPN** and BSA, which is further examined through fluorescence quenching analysis via theoretical and experimental approaches.

3.2. Density functional theory (DFT)

The interaction between a ligand and a protein is largely governed by their electronic properties, which determine their ability to engage in

hydrogen bonding, electrostatic interactions, and charge-transfer processes. In this context, DFT calculations were executed to estimate the electronic structure and global reactivity parameters of **OPN**, with the aim of connecting these properties with its binding behavior towards BSA. The **OPN** molecule structure was fully optimized with the help of the B3LYP/6–31G(d,p) method and presented in Fig. 1. Herein, the B3LYP density functional is used to describe the ground and excited state properties and 6–31G(d,p) basis set is used to calculate the electronic structure of the **OPN** molecule. The frontier molecular orbitals (FMO), including HOMO and LUMO energies, play a significant role in electronic properties and how they interact with various species. A molecule that contains a small energy gap is highly polarized and is said to be a soft molecule, when the energy gap is higher, the molecule is considered to be hard. Fig. 1 shows the HOMO-LUMO energies and energy gaps of the **OPN** molecule. In the visual representation, the red region corresponds to the negative phase, whereas the green regions indicate the positive phase [44].

Moreover, FMO energies are utilized to compute the global reactivity parameters by following the equations [45].

$$\chi = -1/2(E_{HOMO} + E_{LUMO}) \quad (1)$$

$$\mu = -\chi = 1/2(E_{HOMO} + E_{LUMO}) \quad (2)$$

$$\eta = 1/2(E_{HOMO} - E_{LUMO}) \quad (3)$$

$$S = 1/2\eta \quad (4)$$

$$\omega = \mu^2/2\eta \quad (5)$$

The global and local reactivity parameters are presented in Table 2. These parameters help to understand the chemical reactivity, stability and charge transfer ability of the synthesized molecule. The calculated E_{HOMO} (–5.577 eV) and E_{LUMO} (–2.293 eV) values represent the electron-donating and accepting nature of **OPN**. Moreover, the energy gap (ΔE = 3.284 eV) provides the molecule kinetic stability and chemical reactivity [46,47]. The chemical reactivity of an **OPN** compound is strongly governed by its HOMO-LUMO energy gap [48] A smaller energy gap corresponds to lower excitation energy requirements, thereby facilitating electronic transitions and enhancing reactivity and also associated with improved biological activity [49,50]. The HOMO is mainly localized on

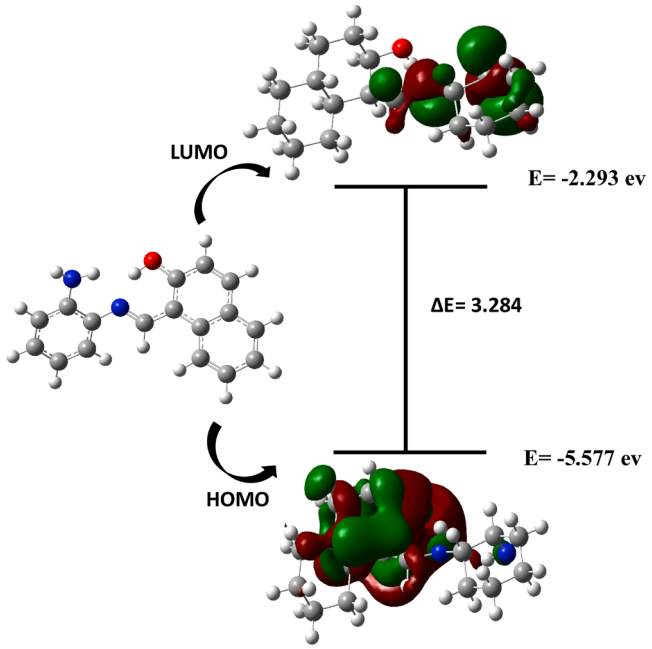

Fig. 1. Optimized structure and HOMO-LUMO energies of **OPN**.

Table 2
Global reactive parameters for **OPN** calculated using DFT.

Global reactive parameters	OPN
E_{HOMO} (ev)	−5.577
E_{LUMO} (ev)	−2.293
Energy gap (ev)	3.284
Ionization energy (IE)	5.577
Electron affinity (EA)	2.293
Electronegativity (χ)	3.935
Chemical potential (μ)	−3.935
Global hardness (η)	1.642
Global softness (s)	0.305
Electrophilicity index (ω)	4.715

the imine nitrogen (C = N) and aromatic π-system, indicating nucleophilic region, whereas the LUMO is distributed over the electron-deficient naphthyl and conjugated backbone, highlighting electrophilic sites [51]. Thus, orbital asymmetry enables dual reactivity and promotes efficient intramolecular charge transfer thereby enhancing overall reactivity and biomolecular potential. For instance, Geetha thamarichelvan et al., reported a Schiff base (NDBDP) and performed DFT studies using B3LYP/6–31G(d,p) method. Their result sowed a HOMO-LMO energy gap of 3.508 eV, indicating moderate stability and reactivity [52]. On the other hand Muhammad Nawaz Tahir et el, reported naphthaldehyde based Schiff base (3,4-DMN and 2,3-DMN) along with detailed structural analysis, where the calculated energy gaps of 3.328 and 3.354 eV indicate that the compounds possess relatively high electronic stability [53]. The ionization energy (IE = 5.577 eV), which represents the energy required to remove an electron from a compound and is related to the corresponding electronic energy level, indicates that **OPN** needs a moderate energy input for electron removal, while the electron affinity (EA = 2.293 eV) confirms its capacity to accept electrons [25].

The comparatively high electronegativity (χ = 3.935 eV) specifies a strong tendency for the molecule to attract electrons, which aligns with the presence of heteroatoms (O and N) in the **OPN** scaffold. The molecule thermodynamic stability largely relies on its chemical potential, suggesting that **OPN** tends to achieve electronic stabilization by accepting electron density from suitable donors. The resistance of the electron cloud to polarization or deformation under slight chemical perturbation is referred to as global hardness. It directly proportional to the energy gap (ΔE), while global softness is inversely related to the energy band gap. The calculate global hardness and softness values indicate that the **OPN** exhibits reasonable resistance to charge transfer, along with improved polarizability, suggesting a favourable interaction with biological targets. Moreover, the **OPN** molecule is effectively involved in nucleophilic-electrophilic interaction, which is confirmed by a strong electrophilic index value. The above-discussed parameters support the potential applicability towards biological applications. Based on these parameter values, **OPN** exhibits increased chemical reactivity, stability, and enhanced polarizability, suggesting a more delocalized electron cloud that can facilitate charge transfer and contribute to increased molecular softness. These electronic properties suggest that **OPN** possesses the necessary reactivity and charge distribution to effectively interact with protein residues. Moreover, the limitation of the present computational analysis is the structural comparison between theoretical and experimental results.

3.3. Interaction between BSA and OPN

Serum albumin is the most abundant protein in the blood and plays critical roles in the body, including drug delivery and transport. Moreover, interaction studies between active drugs, such as ligands, and proteins provide significant insight into their biodistribution, toxicity, and mechanism of action. In this work, we selected BSA as a model protein, because it has a similar structure to HSA [54]. Also, this protein

contains the fluorescent amino acids such as tyrosine, tryptophan, and phenylalanine. Among them, tryptophan exhibits strong fluorescence at 345 nm. Fluorescence spectroscopy is a key method for analyzing structural changes in biomolecules such as membrane components, proteins, and nucleic acids during drug interactions. Due to the strong affinity between proteins and drugs, emission intensities can either increase or decrease. Binding typically reduces emission intensity by altering the fluorophore's environment. In this study, we synthesized a **OPN** and investigated its binding to BSA using absorption and fluorescence techniques. As shown in **Figure S5**, the absorption spectra of BSA remain largely unchanged upon the addition of **OPN**, indicating the absence of significant ground-state complex formation. Fig. 2a illustrates the fluorescence quenching behavior, where BSA exhibits a characteristic emission maximum at 343 nm upon excitation at 285 nm. The concentration of OPN was varied from 0–5 μM, while the BSA concentration was maintained at approximately 15 μM. A progressive decrease in fluorescence intensity was observed with increasing **OPN** concentration. This quenching effect suggests that **OPN** interacts with BSA, altering the microenvironment of aromatic amino acid residues, likely through hydrophobic interactions and potential conformational changes in the protein structure.

The mechanism of fluorescence quenching was analyzed, and the quenching parameters were calculated using the Stern–Volmer (S-V) Eqs. (1a and 2a) [55].

$$I_0/I = 1 + K_{SV}[Q] \quad (1a)$$

$$K_{SV} = k_q \times \tau_0 \quad (2a)$$

Here, I_0 and I denote the fluorescence intensities of the protein in the absence and presence of the analyte, respectively. Additionally, [Q], K_{SV}, and k_q represent the quencher concentration, the Stern-Volmer constant, and the quenching rate constant, respectively. The lifetime (τ_0) of BSA alone is 6 ns. Fig. 2b shows the linear S-V plot, which suggests a dynamic nature of quenching. But sometimes, the static quenching mechanism can also yield a linear plot. The calculated K_{SV}, and k_q are 1.64×10^5 M^{-1} and 2.79×10^{13} M^{-1} s^{-1}, respectively. The obtained k_q value is greater compared to the earlier literature value of dynamic quenching (2.0×10^{10} M^{-1} s^{-1}) [56]. These results support that the quenching process between BSA and **OPN** is static quenching. The results discussed above are insufficient to confirm the quenching mechanism. So, we have performed the fluorescence quenching spectra at various temperatures. **Figure S6** and **2c** show the fluorescence quenching spectra and S-V plot of BSA with OPN at different temperatures. The calculated Ksv and kq values are presented in Table 3. This data clearly revealed that the quenching mechanism between BSA and **OPN** is static, as the calculated K_{sv} decreased with the increasing temperature [57–59].

Double logarithmic Eq. (3a) was used to calculate the binding

Table 3
Fluorescence quenching parameters of BSA with **OPN** at various temperatures.

Compound	K_{SV} ($\times 10^5$ M^{-1})			k_q ($\times 10^{13}$ M^{-1})		
	298 K	303 K	313 K	298 K	303 K	313 K
OPN	1.72	1.56	1.45	2.86	2.60	2.42

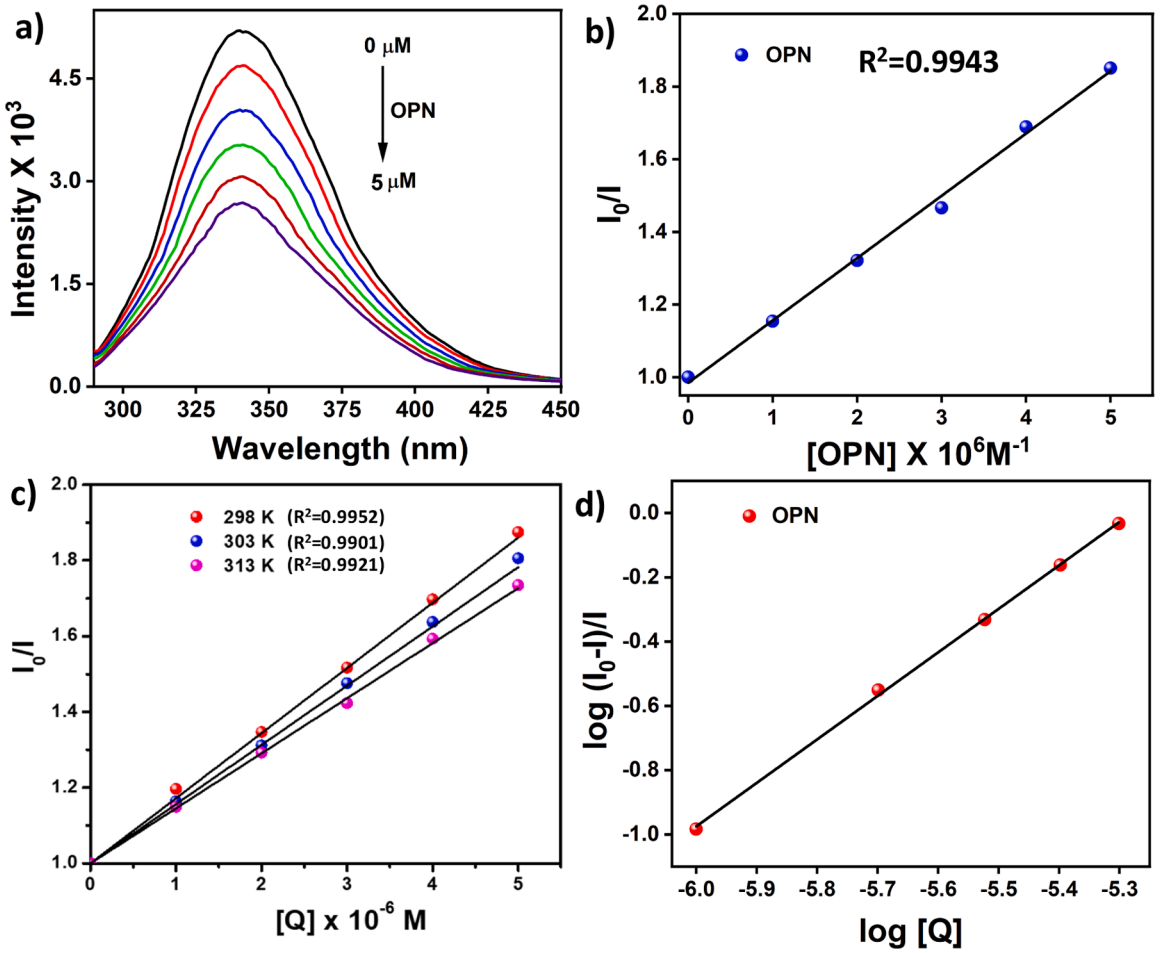

Fig. 2. Fluorescence quenching between BSA and OPN (a) Fluorescence quenching spectra, (b) Stern-Volmer plot against [Q] vs I_0/I, (c) S-V plot at different temperatures, and d) double-logarithmic plot of quenching analysis.

constant (K_b) and number of binding sites (n),

$$\log(I_0-I)/I = \log K_b + n\log(Q) \quad (3a)$$

From the logarithmic plot, K_b and n are calculated using the slope and intercept (Fig. 2d). The calculated values are 7.14×10^5 M^{-1} for K_b and 1 for n, indicating strong binding interactions. This suggests that the binding site is close to 1, indicating that **OPN** binds to BSA in a 1:1 ratio.

The standard Gibbs free energy (ΔG^o) helps to check the spontaneity of the binding process,

$$\Delta G^{\circ} = -RT \ln K_b \quad (4a)$$

Here, R and T represent the gas constant and room temperature, respectively. From Eq. (4), the obtained ΔG^o value is more negative (−39.05 kJ/mol), suggesting the binding interaction is more spontaneous and favourable. To gain molecular level understanding into this interactions, molecular docking studies were performed.

Molecular docking is a useful computational method employed in drug design, commonly used to classify potential drug candidates by analysing their theoretical interactions [60]. Therefore, docking analysis was performed to reveal the binding interactions between **OPN** and BSA. Fig. 3a and b shows the docking results, including interaction data along with the corresponding 2D and 3D images. Docking simulations were carried out for the ligand across 10 conformations, with the best docking chosen based on the lowest binding energy. The moderate binding energy recorded for the **OPN** and BSA complex was −7.7 kcal/mol, showing a stable and robust interaction. The binding site analysis showed that **OPN** interacts with crucial amino acid residues, including LYS-524 via conventional hydrogen bonding and with LEU-574, THR-578, MET-547, LEU-528, VAL-546, LEU-543, and ALA-527 through pi-alkyl and hydrophobic interactions, confirming the formation of a ligand-protein complex.

The interactions of **OPN** with BSA is strongly governed by structural characteristics such as π-conjugation, molecular planarity, and functional group donor. The comparative analysis of previously reported Schiff base analogues with **OPN** highlights how the Schiff base structure modulates binding affinity and docking behaviour. Compared to other naphthalene-based Schiff bases, **OPN** exhibits enhanced protein-binding affinity due to the presence of electron-rich phenolic (–OH) and electron-accepting imine (–C = N–) groups within a conjugated framework, which collectively facilitate strong hydrogen bonding, charge-transfer, and hydrophobic interactions with BSA [57,58,61]. The salicylaldehyde Schiff base, holding a single phenyl ring, shows comparatively lower binding affinity (10^4–10^5 M^{-1}) and lower binding energy (−5.5 to −6.5 kcal/mol). This is due to its inadequate π-surface, which limits π-π stacking interactions within the hydrophobic cavity of BSA [62]. In contrast, compounds incorporating extended aromatic frameworks exhibit enhanced interaction. This trend is supported by binding of a Chromen-4-one Schiff base with BSA, where increase conjugation improves protein affinity [63]. Furthermore, the docking energy of **OPN** is comparable to values reported for Schiff base systems interacting with serum albumin, yet remains slightly less favourable than those observed for metal coordinated complexes. For example, the interaction of Schiff base metal complexes with BSA [64], demonstrated stronger binding (10^4–10^5 M^{-1}; −8 to −9 kcal/mol) due to metal induced rigidity and charge transfer effects. In this context, the relatively moderate binding affinity of **OPN** can be rationalized by its combined structural features, including the presence of naphthalene moiety (enhancing π-π stacking), an imine linkage (facilitating hydrogen bonding), and intramolecular -OH…N interaction (promoting planarity and electronic delocalization). These characteristics enabled **OPN** to attain binding performance superior to simple Schiff bases and comparable to more complex systems, without the need for metal coordination. Overall, the obtained binding energy was −7.7 kcal mol^{-1} specifies a moderate but favorable interaction and is reliable with reported values for small organic Schiff base ligands interacting with BSA.

Moreover, the comparison with structurally related naphthalene Schiff bases (**Table S1**) demonstrates that alterations in donor functional groups, expansion of aromaticity and coordination environments substantially affect BSA binding properties. As compared with other hydroxyl-containing methoxy, nitro and metal ligand derivatives described in literature, **OPN** possesses the novel feature of incorporating a free amine group along with an aromatic hydroxyl group in a mono-naphthalene azomethine group, enabling simultaneous hydrogen-bonding and hydrophobic interactions with BSA.

Further validation was done using docking studies of the binding domains of **OPN** to the BSA in comparison with the already identified site-specific binding markers, warfarin (WF) and ibuprofen (IP). Based on literature data, the binding domains of WF and IP to Site I (subdomain IIA) and Site II (subdomain IIIA) on albumin [65], respectively. In this case, we checked the IP and WF binding sites with BSA through the CB-Dock method (Fig. 4a&b); the docked positions and sites are matched with those previously reported in the literature [66,67]. Moreover, **OPN** docked poses showed at subdomain IIA, this result is similar to warfarin. This agreement confirms the consistency of the docking protocol and supports the accuracy of the predicted binding mode of the inspected ligand with BSA. To further evaluate the molecular stability and reliability of the docked complex, molecular dynamics were performed.

Molecular dynamics simulations are essential for assessing molecular stability during association and conformational changes over time, as

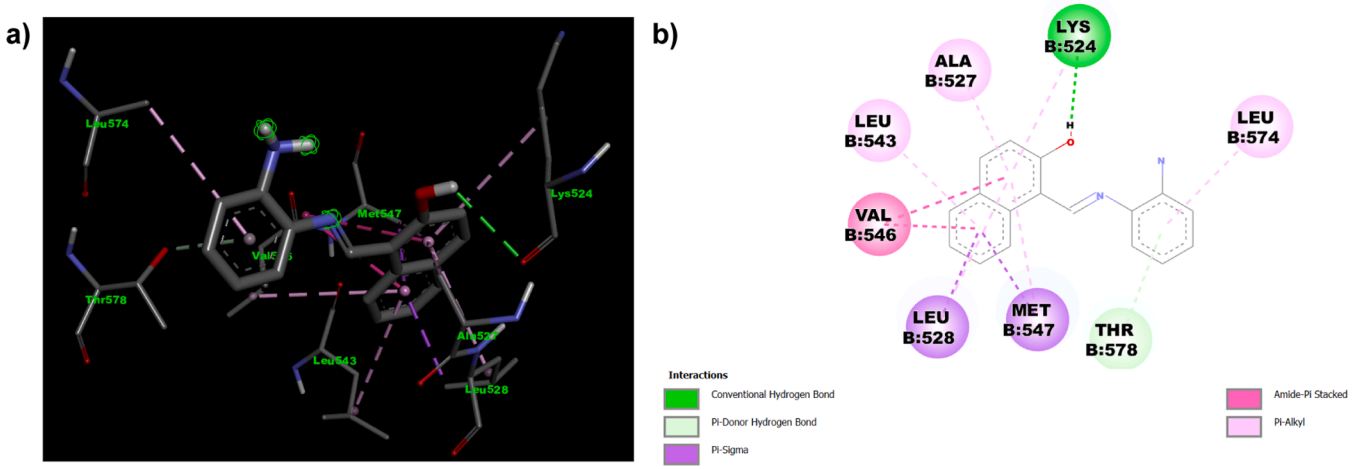

Fig. 3. Molecular docking studies between BSA and **OPN** a) 3D structure and b) 2D structure.

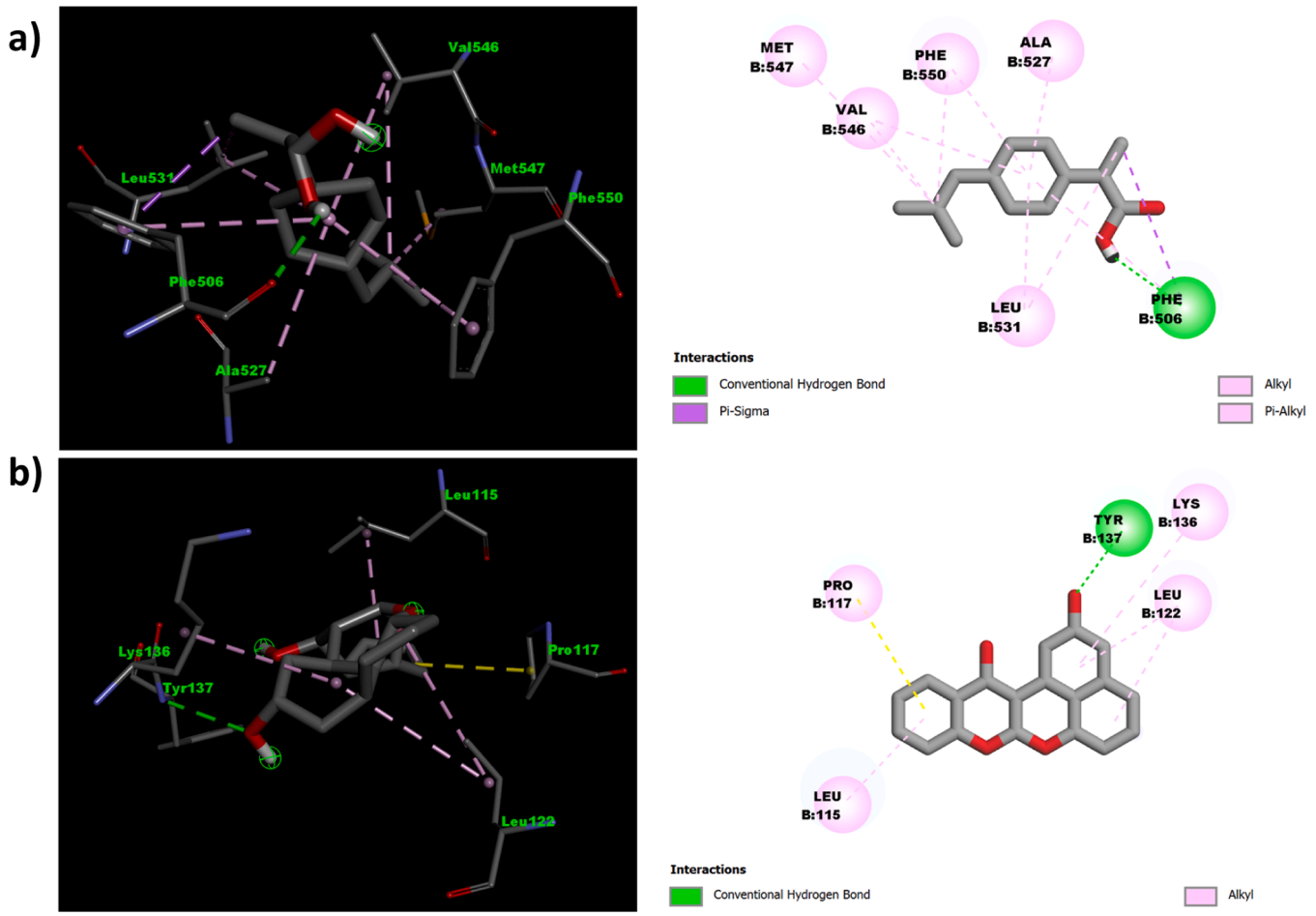

Fig. 4. Docking validation between BSA with a) Ibuprofen and b) Warfarin.

well as for determining the duration of these processes [68]. This method is specifically developed to forecast atomic movements and free binding energy by utilizing different force fields and energy minimization techniques. The predicted values for the protein-ligand complex throughout the simulation indicate overall stability and deviation, based on conformations within the protein's binding site. The time-series line graph shows deviations in nanometres, with the y-axis ranging from 0 to 0.6 nm, and the x-axis shows simulation time (0–50 ns) in nanoseconds. The RMSD profile indicates relative structural accommodation of the protein–ligand complex during the simulation period, although continued fluctuations toward the end of the trajectory suggest ongoing conformational adjustments. Therefore, the present 50 ns simulation provides preliminary evidence of interaction behavior rather than definitive confirmation of full equilibrium stabilization (Fig. 5a). Root-mean-square fluctuation (RMSF) calculations in protein-ligand complexes have been widely used to assess the average positional fluctuations of core atoms around the binding site over the course of a simulation [43,69]. In the scatter line graph, the y-axis shows the magnitude of atomic movements in nanometres (nm), and the x-axis shows the index number of each atom in a protein molecule, ranging

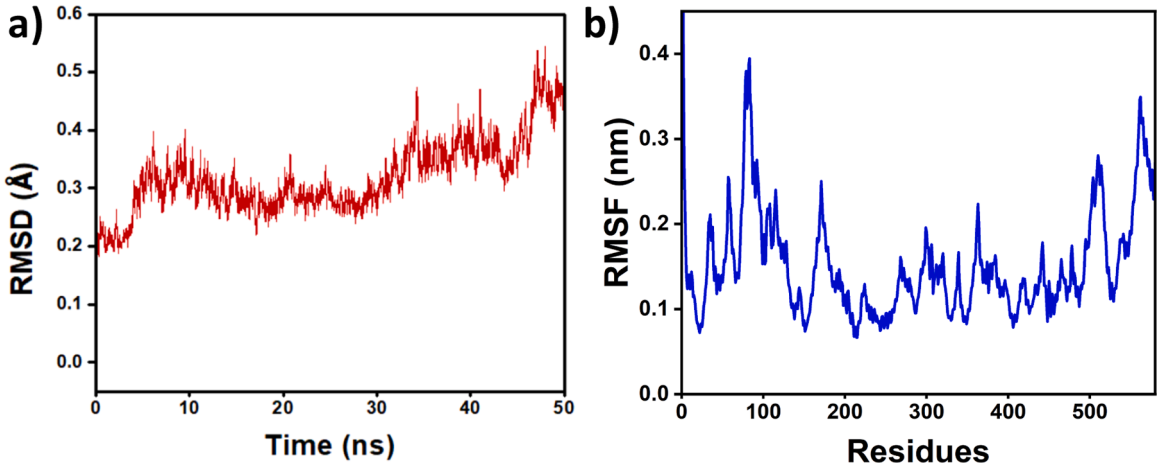

Fig. 5. a) Trajectory analyses of RMSD and b) RMSF were computed using the integrated GROMACS tools.

from 0 to 600. The degree of flexibility is observed through relatively rigid and flexible regions in the system, scaled between 0.1 and 0.4 nm (Fig. 5b). MD simulation analysis showed that the **OPN**-BSA complex is structurally stable and revealed ligand-induced conformational changes in BSA. Overall, the above results provide a primary understanding of protein-ligand interactions, which may be useful for drug design and development. Moreover, we have to perform the following significant analyses in the future, such as longer simulation times, replicate simulations, and additional energetic analyses (MM-PBSA/MM-GBSA), which would provide stronger validation of binding stability.

3.4. Swiss-ADME study

The physicochemical and pharmacological properties of the synthesized ligand will be assessed to anticipate its behaviour in the human body. ADME properties like absorption, distribution, metabolism and excretion offer understanding of how a ligand may be biologically processed, while physicochemical properties like partition coefficient (Log P), molecular weight (MW), and the number of hydrogen donors and acceptors are also vital. These factors help predict a ligand's permeability, potential bioavailability, and overall drug efficacy. Moreover, Lipinski's rule of five provides a helpful guideline for estimating drug-likeness, emphasising the properties mentioned earlier. These rules show that a ligand is more likely to be orally active if it satisfies certain conditions, such as having a Log (<5), MW (<500 Da), fewer than 5 hydrogen bond donors, and ten hydrogen bond acceptors. These characteristics indicate how effectively the **OPN** can cross the cell membrane and maintain pharmacological effects within the body. Fig. 6a and b display the boiled-egg graph and bioavailability radar chart, with the results summarized in Table 4. The bioavailability radar evaluates drug-likeness based on six key physicochemical parameters influencing oral absorption (Fig. 6b). The pink region represents the optimal ranges for each axis and the molecular radar plot must lie entirely within this area to be considered drug-like. The **OPN** compound mostly falls within this zone, with a slight deviation in the saturation, indicating generally favourable drug-like properties.

The obtained Swiss-ADME values are compared with Lipinski's rule of five (Ro5), these values are under acceptable limits, which suggests the molecule shows bioavailability of conventional drugs. Moreover, the molecular weight of the **OPN** is within the range, indicating that it would be readily transported across biological membranes [70]. Similarly, LogP and LogS values are within Lipinski's rule thresholds, indicating that the **OPN** is more lipophilic and soluble in water.

Table 4
Physicochemical and pharmacokinetic properties of the **OPN** compound.

Parameters	OPN	Acceptable threshold (Ro5)
Physicochemical Properties		
Molecular weight (Da)	262.31 g/mol	<500Da
LogP	2.50	<5
LogS(mol/L)	–5.75	(0 to −6)
TPSA	58.61Å	≤140
HBA	2	≤10
HBD	2	≤5
RotBs	2	<10
Consensus $LogP_{o/w}$	3.43	
Pharmacokinetics Properties		
GI absorption	High	
BBB permeant	Yes	
Lipinski	Yes	
Pg-Substrate	No	
$LogK_p$ (skin permeation)	−4.86 cm/s	

Additionally, the topological polar surface area (TPSA) serves an important molecular parameter for predicting drug bioavailability and membrane permeability. The molecule exhibits a TPSA value of 58.61 Å within the acceptable range, suggesting that **OPN** can easily penetrate cells [71]. Other important parameters, such as HBAs, HBDs, and RotBs, help evaluate the suitability of chemical compounds as potential drug candidates. The calculated values remain within Lipinski's rule limits, representing potential bioavailability. Furthermore, the bioavailability score of 0.55 suggests adequate potential for entry into the systemic circulation. For the development of an orally administered drug molecule, efficient intestinal absorption is a crucial criterion for a potential drug candidate. According to the table, **OPN** exhibits high gastrointestinal (GI) absorption, suggesting efficient intestinal uptake, and effective blood-brain barrier (BBB) penetration. This property is a critical factor, particularly for drugs targeting the central nervous system (CNS), as effective therapeutic action requires the ability to cross this barrier [72]. In general, an ideal drug candidate should not bind with P-glycoprotein (P-gp), **OPN** is not a P-gp substrate, suggesting its potential for good bioavailability. Collectively, these findings indicate the strong potential as an orally active drug candidate with favourable absorbability and bioavailability [73]. These pharmacokinetic properties were evaluated using the BOILED-EGG model depicted in Fig. 6a. The skin permeability (Log Kp) value of −4.86 cm/s indicates low transdermal diffusion of **OPN**, as more negative values correspond to reduced permeability. This suggests that it is not favourable for transdermal delivery but is more

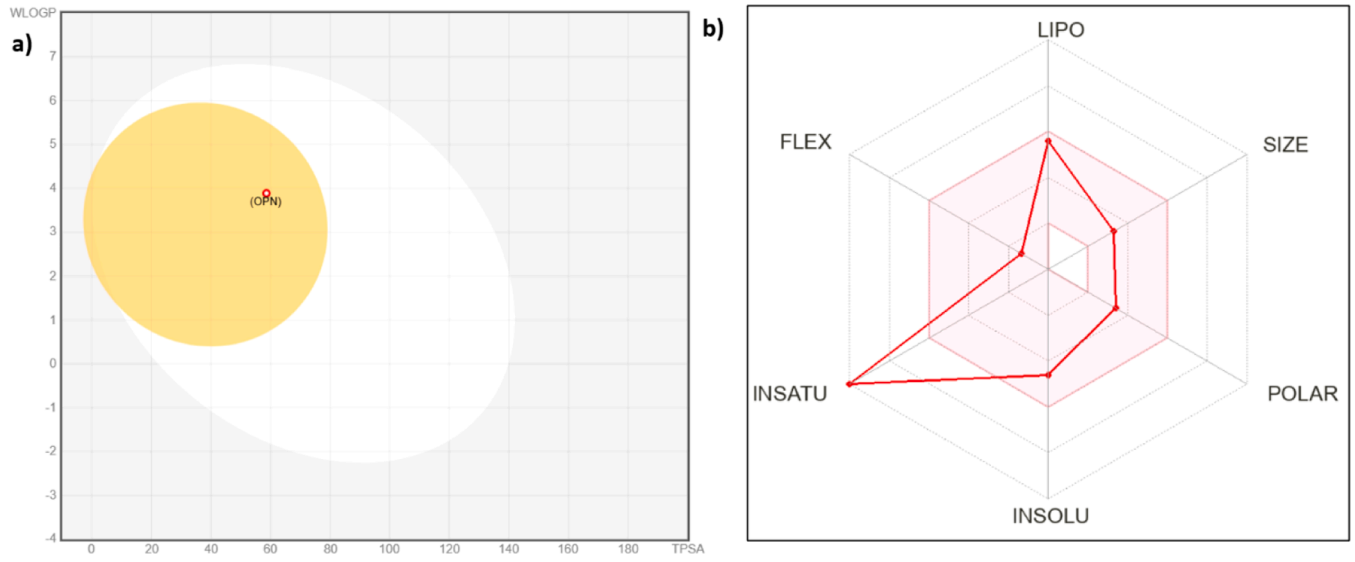

Fig. 6. a) Boiled egg graph representation of **OPN** b) Bioavailability radar chart of physicochemical properties for **OPN**.

suitable for an orally active drug candidate [74]. Overall, the Swiss-ADME analysis supports the conclusion that the **OPN** molecule is a potential drug candidate for further drug development.

4. Conclusion

In this work, we have successfully synthesized the phenolic-based Schiff base ligand, (E)-1-(((2-aminophenyl)imino)methyl)naphthalen-2-ol (**OPN**) from 2-hydroxy-1-naphthaldehyde and o-phenylenediamine. The **OPN** was thoroughly characterized through pivotal spectroscopic techniques like FT-IR, NMR and mass analysis. From DFT calculations of the HOMO-LUMO energy levels and global reactivity parameters, the **OPN** was found to be kinetically stable and highly reactive. Fluorescence quenching analysis showed a strong binding interaction between BSA and **OPN** via static quenching, as evidenced by high values of the quenching rate constant (2.79×10^{13} M^{-1} s^{-1}) and a moderate binding constant (7.14×10^{5} M^{-1}). Molecular docking analysis showed a strong affinity occurred between BSA and **OPN** through hydrogen bonding with LYS 524, and also some electrostatic interactions. The stability of the BSA-**OPN** complex was examined using MD simulations, which showed that the complex remained structurally stable for up to 50 ns. The drug-likeness and pharmacokinetic properties were assessed using SWISS-ADME analysis, which showed that the prepared **OPN** molecule had good bioavailability and a strong tendency to cross the BBB. The drug-likeness and pharmacokinetic properties were assessed using SWISS-ADME analysis, which showed that the prepared **OPN** molecule had good bioavailability and a strong tendency to cross the BBB. Additionally, its interaction with P-gp suggests its potential as a promising drug candidate. Also, the BOILED-Egg model revealed the passive absorption in the gastrointestinal tract and brain penetration (BBB) based on molecular positioning. Furthermore, the calculated bioavailability score (0.55) indicates good drug-likeness. Overall, the synthesized **OPN** provide demonstrated potential as a drug candidate for further pharmaceutical drug development.

CRediT authorship contribution statement

Kathiravan Poornima: Writing – original draft, Software, Data curation. **Venkatesan Srinivasan:** Writing – review & editing, Writing – original draft, Supervision, Software, Resources, Methodology, Investigation, Conceptualization. **Renganathan Senthil:** Software. **Mohandass Yeshwanth Sree:** Software, Data curation. **Pushparaj Sandhyadevi:** Software, Formal analysis. **Kannan Ramamurthy:** Software, Methodology, Formal analysis, Data curation.

Declaration of competing interest

The authors declare that they have no known competing financial interests or personal relationships that could have appeared to influence the work reported in this paper.

Acknowledgements

I gratefully acknowledge the financial support received from Vel Tech Rangarajan Dr. Sagunthala R&D Institute of Science and Technology, under the Seed fund, Grant No. VTU/Seed Fund/FY 2025–-26/018. This support facilitated the successful execution of the research work through the purchase and characterizations of the sample. V.S. also acknowledges the Centre for Molecular Photoscience, Vel Tech Research Park, for the fluorescence measurements.

Supplementary materials

Supplementary material associated with this article can be found, in the online version, at doi:10.1016/j.molstruc.2026.146670.

Data availability

Data will be made available on request.

References

[1] F.K. Bine, N.K. Nkungli, T.S. Numbonui, J.N. Ghogomu, Structural properties and reactive site selectivity of some transition metal complexes of 2,2′(1E,1′E)-(ethane-1,2-diylbis(azan-1-yl-1-ylidene))bis(phenylmethan-1-yl-1-ylidene)dibenzoic acid: DFT, conceptual DFT, QTAIM, and MEP studies, Bioinorg. Chem. Appl. 2018 (2018) 1–11, https://doi.org/10.1155/2018/4510648.

[2] A.K. Manna, K. Rout, S. Chowdhury, G.K. Patra, A dual-mode highly selective and sensitive Schiff base chemosensor for fluorescent colorimetric detection of Ni^{2+} and colorimetric detection of Cu^{2+}, Photochem. Photobiol. Sci. 18 (2019) 1512–1525, https://doi.org/10.1039/c9pp00114j.

[3] A.A. Khandar, F.A. Afkhami, S.A. Hosseini-Yazdi, J.M. White, S. Kassel, W. G. Dougherty, J. Lipkowski, D. Van Derveer, G. Giester, F. Costantino, Anion influence in the structural diversity of cadmium coordination polymers constructed from a pyridine based Schiff base ligand, Inorganica Chim. Acta 427 (2015) 87–96, https://doi.org/10.1016/j.ica.2014.11.028.

[4] A. Kajal, S. Bala, S. Kamboj, N. Sharma, V. Saini, Schiff bases: a versatile pharmacophore, J. Catal. 2013 (2013) 1–14, https://doi.org/10.1155/2013/893512.

[5] M.-J. Kim, R. Konduri, H. Ye, F.M. MacDonnell, F. Puntoriero, S. Serroni, S. Campagna, T. Holder, G. Kinsel, K. Rajeshwar, Dinuclear ruthenium(II) polypyridyl complexes containing large, redox-active, aromatic bridging ligands: synthesis, characterization, and intramolecular quenching of MLCT excited states, Inorg. Chem. 41 (2002) 2471–2476, https://doi.org/10.1021/ic011028u.

[6] M. Sarr, M. Diop, I.E. Thiam, M. Gaye, A.H. Barry, N. Alvarez, J. Ellena, Co-crystal structure of a dinuclear (Zn-Y) and a trinuclear (Zn-Y-Zn) complexes derived from a Schiff base ligand, Eur. J. Chem. 9 (2018) 67–73, https://doi.org/10.5155/eurjchem.9.2.67-73.1688.

[7] M. Matsumoto, K.M. Nicholas, Synthesis of cyclic oligomers from histidine-derived building blocks using dynamic combinatorial chemistry, J. Org. Chem. 72 (2007) 9308–9313, https://doi.org/10.1021/jo701832m.

[8] M. Hajrezaie, P. Hassandarvish, S.Z. Moghadamtousi, N.S. Gwaram, S. Golbabapour, A. NajiHussien, A.A. Almagrami, M. Zahedifard, E. Rouhollahi, H. Karimian, S. Fani, B. Kamalidehghan, N.A. Majid, H.M. Ali, M.A. Abdulla, Chemopreventive evaluation of a schiff base derived copper (II) complex against azoxymethane-induced colorectal cancer in rats, PLoS One 9 (2014) e91246, https://doi.org/10.1371/journal.pone.0091246.

[9] S. Padhyé, G.B. Kauffman, Transition metal complexes of semicarbazones and thiosemicarbazones, Coord. Chem. Rev. 63 (1985) 127–160, https://doi.org/10.1016/0010-8545(85)80022-9.

[10] L. Saghatforoush, K. Moeini, S.A. Hosseini-Yazdi, Z. Mardani, A. Hajabbas-Farshchi, H.T. Jameson, S.G. Telfer, J.D. Woollins, Theoretical and experimental investigation of anticancer activities of an acyclic and symmetrical compartmental Schiff base ligand and its Co(<scp>ii</scp>), Cu(<scp>ii</scp>) and Zn (<scp>ii</scp>) complexes, RSC Adv. 8 (2018) 35625–35639, https://doi.org/10.1039/C8RA07463A.

[11] S. Kasselouri, A. Garoufis, A. Katehanakis, G. Kalkanis, S.P. Perlepes, N. Hadjiliadis, 1:1 Metal complexes of 2-(2′-pyridyl)quinoxaline, a ligand unexpectedly formed by the reaction between 2-acetylpyridine and 1,2-phenylenediamine, Inorganica Chim. Acta 207 (1993) 255–258, https://doi.org/10.1016/S0020-1693(00)90718-7.

[12] D. Sinha, A.K. Tiwari, S. Singh, G. Shukla, P. Mishra, H. Chandra, A.K. Mishra, Synthesis, characterization and biological activity of Schiff base analogues of indole-3-carboxaldehyde, Eur. J. Med. Chem. 43 (2008) 160–165, https://doi.org/10.1016/j.ejmech.2007.03.022.

[13] W. Villarreal, L. Colina-Vegas, G. Visbal, O. Corona, R.S. Corrêa, J. Ellena, M. R. Cominetti, A.A. Batista, M. Navarro, Copper(I)–Phosphine polypyridyl complexes: synthesis, characterization, DNA/HSA binding study, and antiproliferative activity, Inorg. Chem. 56 (2017) 3781–3793, https://doi.org/10.1021/acs.inorgchem.6b02419.

[14] S. Adsule, V. Barve, D. Chen, F. Ahmed, Q.P. Dou, S. Padhye, F.H. Sarkar, Novel schiff base copper complexes of quinoline-2 carboxaldehyde as proteasome inhibitors in Human prostate cancer cells, J. Med. Chem. 49 (2006) 7242–7246, https://doi.org/10.1021/jm060712l.

[15] J. Kruk, B.H. Aboul-Enein, E. Duchnik, M. Marchlewicz, Antioxidative properties of phenolic compounds and their effect on oxidative stress induced by severe physical exercise, J. Physiol. Sci. 72 (2022) 19, https://doi.org/10.1186/s12576-022-00845-1.

[16] S. Soares, N. Mateus, V. de Freitas, Interaction of different polyphenols with bovine serum albumin (BSA) and Human salivary α-amylase (HSA) by fluorescence quenching, J. Agric. Food Chem. 55 (2007) 6726–6735, https://doi.org/10.1021/jf070905x.

[17] M.B. ELLIOTT, P.A. GOTTLIEB, P. GOLLNICK, The mechanism of RNA binding to TRAP: initiation and cooperative interactions, RNA 7 (2001) 85–93, https://doi.org/10.1017/S135583820100173X. S135583820100173X.

[18] L. Que, W.B. Tolman, Biologically inspired oxidation catalysis, Nature 455 (2008) 333–340, https://doi.org/10.1038/nature07371.

[19] J. Hao, Y. Zhang, X. Wang, H. Yan, E. Liu, X. Gao, Interaction between the natural components in Danhong injection (DHI) with serum albumin (SA) and the influence of the coexisting multi-components on the SaB-BSA binding system:

fluorescence and molecular docking studies, PLoS One 10 (2015) e0128919, https://doi.org/10.1371/journal.pone.0128919.
[20] P. Cui, M. Cai, Y. Meng, Y. Yang, H. Song, Y. Liu, Q. Wang, Design, synthesis and biological activities of echinopsine derivatives containing acylhydrazone moiety, Sci. Rep. 12 (2022) 2935, https://doi.org/10.1038/s41598-022-06775-7.
[21] A. Papadopoulou, R.J. Green, R.A. Frazier, Interaction of flavonoids with bovine serum albumin: a fluorescence quenching study, J. Agric. Food Chem. 53 (2005) 158–163, https://doi.org/10.1021/jf048693g.
[22] A.M. Alanazi, A.H. Bakheit, M.W. Attwa, A.S. Abdelhameed, Spectroscopic, molecular docking and dynamic simulation studies of binding between the new anticancer agent olmutinib and human serum albumin, J. Biomol. Struct. Dyn. 40 (2022) 14236–14246, https://doi.org/10.1080/07391102.2021.2001380.
[23] F. Alam, M. Ismail, M. Kamal, F. Ur Rahman, A. Alam, A.F. AlAsmari, F. Alasmari, M. Khan, Investigating the tyrosinase inhibitory activity of 4-bromobenzoic acid hydrazone-Schiff bases, in: Vitro, Molecular Structure and Docking Studies, ChemistrySelect, 9, 2024, https://doi.org/10.1002/slct.202401987.
[24] A. Shakoor, A. Alam, M. Ali, S. Ullah, S.A. Halim, M.U. Rehman, A.F. AlAsmari, F. Alasmari, A. Khan, M. Khan, A. Al-Harrasi, Synthesis of novel benzimidazole analogs for neurodegenerative diseases by targeting prolyl oligopeptidase, ChemistrySelect 9 (2024), https://doi.org/10.1002/slct.202401904.
[25] A. Shakoor, F. Jan, S. Rahman, M. Ali, M. Ibrahim, H. Khan, A. Alam, A. Khan, A. Ali, E. Al-Olayan, M.R. Abukhadra, A. Al-Harrasi, M. Khan, Synthesis, urease inhibitory activity, molecular docking, dynamics, MMGBSA and DFT studies of hydrazone-schiff bases bearing benzimidazole scaffold, Chem. Biodivers. 22 (2025), https://doi.org/10.1002/cbdv.202402096.
[26] X. Chen, Y. Xiang, A. Tong, Facile, sensitive and selective fluorescence turn-on detection of HSA/BSA in aqueous solution utilizing 2,4-dihydroxyl-3-iodo salicylaldehyde azine, Talanta 80 (2010) 1952–1958, https://doi.org/10.1016/j.talanta.2009.10.053.
[27] X. Xu, J. Huang, J. Li, J. Yan, J. Qin, Z. Li, A graphene oxide-based AIE biosensor with high selectivity toward bovine serum albumin, Chem. Commun. 47 (2011) 12385, https://doi.org/10.1039/c1cc15735c.
[28] J.R. Lakowicz (Ed.), Principles of Fluorescence Spectroscopy, Springer US, Boston, MA, 2006, https://doi.org/10.1007/978-0-387-46312-4.
[29] D.C. Carter, J.X. Ho, Structure of serum albumin, in: 1994: pp. 153–203. https://doi.org/10.1016/S0065-3233(08)60640-3.
[30] H.F. Crouse, J. Potoma, F. Nejrabi, D.L. Snyder, B.S. Chohan, S. Basu, Quenching of tryptophan fluorescence in various proteins by a series of small nickel complexes, Dalton Trans. 41 (2012) 2720, https://doi.org/10.1039/c2dt12169g.
[31] S. Radisavljević, A. Đeković Kesić, D. Ćoćić, R. Puchta, L. Senft, M. Milutinović, N. Milivojević, B. Petrović, Studies of the stability, nucleophilic substitution reactions, DNA/BSA interactions, cytotoxic activity, DFT and molecular docking of some tetra- and penta-coordinated gold(<scp>iii</scp>) complexes, New J. Chem. 44 (2020) 11172–11187, https://doi.org/10.1039/D0NJ02037K.
[32] S. Sugio, A. Kashima, S. Mochizuki, M. Noda, K. Kobayashi, Crystal structure of human serum albumin at 2.5 Å resolution, Protein Eng. Des. Selection 12 (1999) 439–446, https://doi.org/10.1093/protein/12.6.439.
[33] J. Flarakos, K.L. Morand, P. Vouros, High-throughput solution-based medicinal library screening against Human serum albumin, Anal. Chem. 77 (2005) 1345–1353, https://doi.org/10.1021/ac048685z.
[34] S. Chakraborti, P. Joshi, D. Chakravarty, V. Shanker, Z.A. Ansari, S.P. Singh, P. Chakrabarti, Interaction of polyethyleneimine-functionalized ZnO nanoparticles with bovine serum albumin, Langmuir 28 (2012) 11142–11152, https://doi.org/10.1021/la3007603.
[35] N.A. Kratochwil, W. Huber, F. Müller, M. Kansy, P.R. Gerber, Predicting plasma protein binding of drugs: a new approach, Biochem. Pharmacol. 64 (2002) 1355–1374, https://doi.org/10.1016/S0006-2952(02)01074-2.
[36] S. Rashidipour, S. Naeeminejad, J. Chamani, Study of the interaction between DNP and DIDS with human hemoglobin as binary and ternary systems: spectroscopic and molecular modeling investigation, J. Biomol. Struct. Dyn. 34 (2016) 57–77, https://doi.org/10.1080/07391102.2015.1009946.
[37] Z. Sharif-Barfeh, S. Beigoli, S. Marouzi, A.S. Rad, A. Asoodeh, J. Chamani, Multi-spectroscopic and HPLC studies of the interaction between estradiol and cyclophosphamide with Human serum albumin: binary and ternary systems, J. Solution. Chem. 46 (2017) 488–504, https://doi.org/10.1007/s10953-017-0590-2.
[38] M. Kabiri, Z. Amiri-Tehranizadeh, A. Baratian, M.R. Saberi, J. Chamani, Use of spectroscopic, zeta potential and molecular dynamic techniques to study the interaction between Human holo-transferrin and two antagonist drugs: comparison of binary and ternary systems, Molecules 17 (2012) 3114–3147, https://doi.org/10.3390/molecules17033114.
[39] G. Gece, The use of quantum chemical methods in corrosion inhibitor studies, Corros. Sci. 50 (2008) 2981–2992, https://doi.org/10.1016/j.corsci.2008.08.043.
[40] M. Anjomshoa, S.J. Fatemi, M. Torkzadeh-Mahani, H. Hadadzadeh, DNA- and BSA-binding studies and anticancer activity against human breast cancer cells (MCF-7) of the zinc(II) complex coordinated by 5,6-diphenyl-3-(2-pyridyl)-1,2,4-triazine, Spectrochim. Acta A Mol. Biomol. Spectrosc. 127 (2014) 511–520, https://doi.org/10.1016/j.saa.2014.02.048.
[41] B. Hess, C. Kutzner, D. van der Spoel, E. Lindahl, GROMACS 4: algorithms for highly efficient, load-balanced, and scalable molecular simulation, J. Chem. Theory. Comput. 4 (2008) 435–447, https://doi.org/10.1021/ct700301q.
[42] S. Ramalakshmi, S. Sathyapriya, R. Senthil, T. Anand, K.M. Saravanan, Integrating deep learning and molecular dynamics to identify GPR17 ligands for glioblastoma therapy, Curr. Chem. Biol. 19 (2025) 38–49, https://doi.org/10.2174/0122127968351148241129071716.
[43] K. Saravanan, R. Senthil, PreFRP: prediction and visualization of fluctuation residues in proteins, J. Nat. Sci. Biol. Med. 7 (2016) 124, https://doi.org/10.4103/0976-9668.184696.
[44] R. Rijal, H.P. Lamichhane, K. Pudasainee, Molecular structure, homo-lumo analysis and vibrational spectroscopy of the cancer healing pro-drug temozolomide based on dft calculations, AIMS Biophys. 9 (2022) 208–220, https://doi.org/10.3934/biophy.2022018.
[45] R. Rijal, M. Sah, H.P. Lamichhane, Molecular simulation, vibrational spectroscopy and global reactivity descriptors of pseudoephedrine molecule in different phases and states, Heliyon 9 (2023) e14801, https://doi.org/10.1016/j.heliyon.2023.e14801.
[46] F.H. Al-Ostoot, D.V. Geetha, Y.H.E. Mohammed, P. Akhileshwari, M.A. Sridhar, S. A. Khanum, Design-based synthesis, molecular docking analysis of an anti-inflammatory drug, and geometrical optimization and interaction energy studies of an indole acetamide derivative, J. Mol. Struct. 1202 (2020) 127244, https://doi.org/10.1016/j.molstruc.2019.127244.
[47] D.F.V. Lewis, C. Ioannides, D.V. Parke, Interaction of a series of nitriles with the alcohol-inducible isoform of P450: computer analysis of structure—Activity relationships, Xenobiotica 24 (1994) 401–408, https://doi.org/10.3109/00498259409043243.
[48] A.-A.M. Al-Dies, F.F. Alblewi, R.M. Okasha, M.H. Alsehli, R.M.A. Borik, S. Ihmaid, A.E.-G.E. Amr, H.A. Ghabbour, A.A. Elhenawy, A.M. El-Agrody, Synthesis, crystal structure, hirshfeld study, DFT analysis, molecular docking study, antimicrobial activity of β-enaminonitrile bearing 1H-pyran, Discover Appl. Sci. 7 (2025) 71, https://doi.org/10.1007/s42452-024-06254-w.
[49] L.P. Ding, F.H. Zhang, Y.S. Zhu, C. Lu, X.Y. Kuang, J. Lv, P. Shao, Understanding the structural transformation, stability of medium-sized neutral and charged silicon clusters, Sci. Rep. 5 (2015) 15951, https://doi.org/10.1038/srep15951.
[50] M.A. Raza, M.W. Mumtaz, S. Öztürk, M. Latif, A.A. Aisha, N. Dege, O.E. Dogan, E. Agar, S.U. Rehman, A. Noor, Experimental and theoretical biological probing of schiff bases as esterase inhibitors: structural, spectral and molecular insights, Molecules 28 (2023) 5703, https://doi.org/10.3390/molecules28155703.
[51] Y. Huang, C. Rong, R. Zhang, S. Liu, Evaluating frontier orbital energy and HOMO/LUMO gap with descriptors from density functional reactivity theory, J. Mol. Model. 23 (2017) 3, https://doi.org/10.1007/s00894-016-3175-x.
[52] G. Thamaraichelvan, Characterisation Synthesis, DFT studies and electrochemical and biological application studies of a new schiff base based on from naphthalene-1, 8-diamine and its Co(II), Ni(II), Cu(II) and Zn(II) complexes, Orient. J. Chem. 40 (2024) 1786–1795, https://doi.org/10.13005/ojc/400631.
[53] M.N. Tahir, M. Ashfaq, Z. Rashid, K.S. Munawar, S. Andleeb, N. Egor, S. Batool, N. Tariq, Synthesis, single-crystal X-ray structural elucidation, and computational and molecular docking studies of naphthaldehyde-based schiff bases, J. Mol. Struct. 1364 (2026) 145914, https://doi.org/10.1016/j.molstruc.2026.145914.
[54] X.-L. Han, P. Mei, Y. Liu, Q. Xiao, F.-L. Jiang, R. Li, Binding interaction of quinclorac with bovine serum albumin: a biophysical study, Spectrochim. Acta A Mol. Biomol. Spectrosc. 74 (2009) 781–787, https://doi.org/10.1016/j.saa.2009.08.018.
[55] S. Gurusamy, M. Sankarganesh, V. Sathish, K. Rajakumar, A. Mathavan, Fluorescence chemosensor for anion recognition, solvatochromism and protein binding studies based on Schiff- base derivative, J. Mol. Struct. 1312 (2024) 138542, https://doi.org/10.1016/j.molstruc.2024.138542.
[56] H. Al Shmrany, A. Alqahtani, T. Alqahtani, A. Alshehri, A.A. Almrasy, Sustainable spectrofluorimetric determination of berberine in dietary supplements via Erythrosin B ion-Pair complexation with mechanistic investigation, Box-Behnken optimization, and green chemistry assessment, Sci. Rep. 16 (2026) 4712, https://doi.org/10.1038/s41598-026-36903-6.
[57] A. Saber Abdelhameed, A.H. Bakheit, E.S. Hassan, A.M. Alanazi, A.M. Naglah, H. AlRabiah, Spectroscopic and computational investigation of the interaction between the new anticancer agent enasidenib and human serum albumin, Spectrochim. Acta A Mol. Biomol. Spectrosc. 270 (2022) 120790, https://doi.org/10.1016/j.saa.2021.120790.
[58] A. Abdelhameed, A. Bakheit, M. Mohamed, W. Eldehna, H. Abdel-Aziz, M. Attia, Synthesis and biophysical insights into the binding of a potent anti-proliferative non-symmetric bis-isatin derivative with bovine serum albumin: spectroscopic and molecular docking approaches, Appl. Sci. 7 (2017) 617, https://doi.org/10.3390/app7060617.
[59] J. Zhang, Q. Yan, J. Liu, X. Lu, Y. Zhu, J. Wang, S. Wang, Study of the interaction between 5-sulfosalicylic acid and bovine serum albumin by fluorescence spectroscopy, J. Lumin. 134 (2013) 747–753, https://doi.org/10.1016/j.jlumin.2012.06.053.
[60] S. Shamim, R. Munawar, Y. Rashid, S. Muhammad Zesshan Qadar, R. Bushra, I. Begum, M. Imran, T. Quds, Molecular docking: an insight from drug discovery to drug repurposing approach, in: 2024. https://doi.org/10.5772/intechopen.1005526.
[61] N. Joksimović, J. Petronijević, D. Ćoćić, N. Janković, E. Milović, M. Kosanić, N. Petrović, Synthesis, characterization, biological evaluation, BSA binding properties, density functional theory and molecular docking study of Schiff bases, J. Mol. Struct. 1244 (2021) 130952, https://doi.org/10.1016/j.molstruc.2021.130952.
[62] A.V. Afonin, D.V. Pavlov, A.V. Vashchenko, Case study of 2-vinyloxypyridine: quantitative assessment of the intramolecular C H···N hydrogen bond energy and its contribution to the one-bond 13C1H coupling constant, J. Mol. Struct. 1176 (2019) 73–85, https://doi.org/10.1016/j.molstruc.2018.08.050.
[63] S. Chandrasekaran, N. Sudha, D. Premnath, I.V.M.V. Enoch, Binding of a chromen-4-one Schiff's base with bovine serum albumin: capping with β-cyclodextrin

influences the binding, J. Biomol. Struct. Dyn. 33 (2015) 1945–1956, https://doi.org/10.1080/07391102.2014.980323.
[64] H. Dezhampanah, M. Esmaili, S. Jampour, Spectroscopic and molecular docking studies on interaction of two Schiff base complexes with bovine serum albumin, J. Biomol. Struct. Dyn. 38 (2020) 2650–2658, https://doi.org/10.1080/07391102.2019.1639548.
[65] D. Leckband, Measuring the forces that control protein interactions, Annu. Rev. Biophys. Biomol. Struct. 29 (2000) 1–26, https://doi.org/10.1146/annurev.biophys.29.1.1.
[66] B. Dkhar, A. Arunkumar, V. Rajendiran, V. Srinivasan, V. Lavanya, M. Velusamy, Copper(I) complexes of triazine- based ligands: synthesis, crystal structure and biological applications, J. Mol. Struct. 1350 (2026) 144042, https://doi.org/10.1016/j.molstruc.2025.144042.
[67] L. Nguyen, L. Hicks, L. Jodoin, S. Carby, D.S. Sanford, A. Mishra, R. Yadav, Investigating quinclorac binding to Human serum albumin using spectroscopy and molecular docking, (2026). https://doi.org/10.64898/2026.01.08.698511.
[68] K.M. Saravanan, H. Zhang, R. Senthil, K.K. Vijayakumar, V. Sounderrajan, Y. Wei, H. Shakila, Structural basis for the inhibition of SARS-CoV2 main protease by Indian medicinal plant-derived antiviral compounds, J. Biomol. Struct. Dyn. 40 (2022) 1970–1978, https://doi.org/10.1080/07391102.2020.1834457.
[69] K.M. Saravanan, H. Zhang, R. Senthil, K.K. Vijayakumar, V. Sounderrajan, Y. Wei, H. Shakila, Structural basis for the inhibition of SARS-CoV2 main protease by Indian medicinal plant-derived antiviral compounds, J. Biomol. Struct. Dyn. 40 (2022) 1970–1978, https://doi.org/10.1080/07391102.2020.1834457.
[70] S.A. Abdel-Latif, A.A. Mohamed, Synthesis, spectroscopic characterization, first order nonlinear optical properties and DFT calculations of novel Mn(II), Co(II), Ni (II), Cu(II) and Zn(II) complexes with 1,3-diphenyl-4-phenylazo-5-pyrazolone ligand, J. Mol. Struct. 1153 (2018) 248–261, https://doi.org/10.1016/j.molstruc.2017.10.002.
[71] P. Babaei, V.H. Rezvan, N.S. Gilani, S.R. Mansour, Molecular docking and in vitro biological studies of a Schiff base ligand as anticancer and antibacterial agents, Results Chem. 7 (2024) 101517, https://doi.org/10.1016/j.rechem.2024.101517.
[72] F.M.G. Cornelissen, G. Markert, G. Deutsch, M. Antonara, N. Faaij, I. Bartelink, D. Noske, W.P. Vandertop, A. Bender, B.A. Westerman, Explaining blood–Brain barrier permeability of small molecules by integrated analysis of different transport mechanisms, J. Med. Chem. 66 (2023) 7253–7267, https://doi.org/10.1021/acs.jmedchem.2c01824.
[73] J.H. Lin, M. Yamazaki, Role of P-glycoprotein in pharmacokinetics, Clin. Pharmacokinet. 42 (2003) 59–98, https://doi.org/10.2165/00003088-200342010-00003.
[74] A. Daina, O. Michielin, V. Zoete, SwissADME: a free web tool to evaluate pharmacokinetics, drug-likeness and medicinal chemistry friendliness of small molecules, Sci. Rep. 7 (2017) 42717, https://doi.org/10.1038/srep42717.